

Article

PLLA/Graphene Nanocomposites Membranes with Improved Biocompatibility and Mechanical Properties

Yaoting He ¹, Jiafei Yan ², Xuzhao He ¹, Wenjian Weng ¹ and Kui Cheng ^{1,*}

¹ School of Materials Science and Engineering, State Key Laboratory of Silicon Materials, Center of Rehabilitation Biomedical Materials, Cyrus Tang Center for Sensor Materials and Applications, Zhejiang University, Hangzhou 310027, China; 22026060@zju.edu.cn (Y.H.); hf@zju.edu.cn (X.H.); wengwj@zju.edu.cn (W.W.)

² The Affiliated Sir Run Run Shaw Hospital of Medical College, Zhejiang University, Hangzhou 310016, China; yan_jiafei@163.com

* Correspondence: chengkui@zju.edu.cn; Tel.: +86-0571-8795-3945

Abstract: In this work, nanocomposite membranes based on graphene and polylactide were evaluated for mechanical properties and biocompatibility. Single-layer graphene (SLG), graphene nanosheets (GNS), and poly L-lactic acid (PLLA) were prepared through layer-by-layer deposition and homogeneous mixing. The results revealed that PLLA/SLG nanocomposites and PLLA/GNS nanocomposites could show enhanced mechanical properties and biocompatibility. The addition of a tiny amount of SLG significantly improved Young's modulus and tensile strength of the PLLA matrix by 15.9% and 32.8% respectively, while the addition of the same mass ratio of GNS boosted the elongation at break of the PLLA matrix by 79.7%. These results were ascribed to the crystallinity and interfacial interaction differences resulting from graphene incorporation. Also, improved biocompatibility was observed with graphene incorporation. Such nanocomposites membranes showed a lot of potential as environment-friendly and biomedical materials.

Keywords: single-layer graphene; mechanical properties; thermal stability; biocompatibility



Citation: He, Y.; Yan, J.; He, X.; Weng, W.; Cheng, K. PLLA/Graphene Nanocomposites Membranes with Improved Biocompatibility and Mechanical Properties. *Coatings* **2022**, *12*, 718. <https://doi.org/10.3390/coatings12060718>

Academic Editor: Giorgos Skordaris

Received: 29 April 2022

Accepted: 19 May 2022

Published: 24 May 2022

Publisher's Note: MDPI stays neutral with regard to jurisdictional claims in published maps and institutional affiliations.



Copyright: © 2022 by the authors. Licensee MDPI, Basel, Switzerland. This article is an open access article distributed under the terms and conditions of the Creative Commons Attribution (CC BY) license (<https://creativecommons.org/licenses/by/4.0/>).

1. Introduction

Biodegradable polymers attract more and more attention in many biomedical and environmental areas. As a typical biodegradable polymer, polylactic acid (PLA) is a polyester material with superior optical, physical, mechanical, and barrier properties, PLA has been widely used in the production of environment-friendly food packaging as freestanding membranes or coatings [1–4] and has great potential as a sustainable alternative to petrochemical-derived polymers [5]. In addition, PLA has also played a great role in advancing the development of biomedical materials due to its superior biocompatibility and degradability. Currently, sutures, stents, orthopedic implants, and drug delivery systems produced from polylactic acid and other biodegradable polymers have mature clinical applications [6–9].

However, rather poor tensile strength and weak impact toughness owing to the amorphous or semi-crystalline structure of PLA limited its application. Normal technical methods are found to be difficult to increase these crystalline characteristics [10,11]. Hence, modification of PLA becomes one of the research focuses. The mechanical characteristics and thermal stability of PLA have been improved using a variety of techniques. One of the most efficient ways to enhance the crystallization characteristics of PLA is to use nanofillers as nucleating agents to lower the nucleation activation energy [12–17]. Therefore, a variety of high-performance nano-reinforcing agents such as nanoclays, nanofibers, carbon nanotubes, etc. were developed [18–22].

Graphene is a nanomaterial with one-atom-thick carbon atoms arranged in a two-dimensional honeycomb structure. Since the first separation of graphene by Navoselov

in 2004 [23], graphene has sparked the extensive interest of scientists in various fields due to its unique physical and chemical properties, including ultra-high specific surface area, exceptional electrical, thermal, and mechanical properties [24–26]. At the same time, these properties make graphene an ideal nano-enhancer, and some composite materials with higher comprehensive properties have been obtained [27–29]. It is noteworthy that the reinforcing impact of nanofillers like graphene in polymers is heavily reliant on their efficient interfacial interaction with the polymer matrix [30,31]. In general, the larger the contact area of the nanofiller with the polymer matrix, the better the dispersion and the performance of composites. Considering the application requirements of biomedical materials, the good biocompatibility of nanofillers is essential. The response of living cells to the graphene-filled polymer nanomaterials depends greatly on the properties of graphene such as layer number, lateral size, purity, dose, surface chemistry, and hydrophilicity. Therefore, the selection of nanofillers as reinforcing agents usually requires consideration of several factors including the surface area, type, structure, and biocompatibility of the filler [32].

Presently, numerous experiments and theoretical studies have been conducted on the PLA composites of graphene and modified graphene [33–35]. Nonetheless, research on single-layer graphene (SLG) and graphene nanosheets (GNS)-filled PLA composite materials is still in its early stages. This is primarily because the compounding of PLA with SLG based on completely preserving the properties of SLG is still challenging. Despite this, as a material that can enhance the ability of human osteogenic differentiation [36], the performance and prospective biomedical applications of SLG and GNS in PLA composites cannot be underestimated.

In this article, the impacts and properties of SLG and GNS in poly L-lactic acid (PLLA) nanocomposites are compared. The effects of the different interactions between SLG/GNS and PLLA were elucidated by a direct comparison of various properties of the two composites using the same preparation methods and process parameters. The tensile properties and fracture toughness of SLG and GNS-filled PLLA nanocomposites were investigated. The biocompatibility of the nanocomposites was also studied.

2. Materials and Experimental Procedure

2.1. Preparation of PLLA/SLG Films

The PLLA/SLG films were prepared following the method described in the literature [37]. Briefly, a single-layer Gr (Xianfeng Nanomaterials, Nanjing, China) grown on a Cu substrate by CVD was spin-coated with 20–30 mg/mL PLLA solution (Huanuo Biomaterials, Changchun, China, the solvent was dichloride methane, molecular weight 200,000). The spin-coated polymer film was dried at room temperature for 2 h to completely evaporate the solvent. Then, the copper substrate was etched away with an aqueous ammonium persulfate solution (Aladdin Chemical Reagent, 0.1 M, Wokai Biotechnology Co., Ltd., Shanghai, China) for less than 8 h. After the copper sheet was completely etched, slowly rinse the PLLA/SLG film with deionized water more than 4 times.

2.2. Fabrication of PLLA/SLG and PLLA/GNS Composites

The composites were prepared by the solution casting method. Using a film applicator to flatly and evenly cover the PLLA surface of the PLLA/SLG film with the 50 mg/mL PLLA solution (the solvent was 1,4-dioxane), cut the obtained PLLA/SLG (PSG) film into desired shapes after drying for 24 h. The mass ratio of PLA to monolayer graphene ($M_{\text{PLLA}}/M_{\text{Graphene}}$) in PSG composite films was calculated. Then, graphene nanosheets (GNS, Shanghai Pro-Graphene, Shanghai, China) containing the same $M_{\text{PLLA}}/M_{\text{Graphene}}$ were dispersed in 50 mg/mL PLLA solution to obtain PLLA/GNS solution. The PLLA/GNS solution was uniformly spread into a film with the same thickness parameters using the film applicator and then dried in an oven at 37 °C for 24 h to obtain composite films of PLLA/GNS (PGN).

2.3. Analysis and Characterization

Raman spectra were taken on samples to characterize the chemical components and structure of SLG and GNS using Micro-Raman (Renishaw plc, inVia-Reflex, NT-MDT Co., Moscow, Russia) with a DXR laser operating at 532 nm. X-ray diffraction (XRD) measurement was conducted by an X'pert PRO (PANalytical B.V., Almelo, The Netherlands) X-ray diffractometer at room temperature. The diffracted intensity of Cu K α radiation ($k = 1.54178 \text{ \AA}$) was recorded with a scanning speed of $5^\circ/\text{min}$ from 10° to 80° . The surface morphology of composites was observed with scanning electron microscopy (SEM, S-4800, SU-70 Hitachi, Tokyo, Japan).

The mechanical properties of composites were tested by using a tensile machine (Zwick GmbH&Co.KG, Z005, Dongguan, China) at a crosshead speed of $5 \text{ mm}/\text{min}$ at room temperature. The samples were cut into rectangular shapes of 5 mm wide and 20 mm long. The reported tensile strength and elongation at break were the average values of at least four samples. Crystallization evolution was observed using an E600POL polarizing microscope (POM, NIKON, Japan). To imitate the crystallization behavior during the fabrication process of composites, the melted samples were cooled to room temperature at $80^\circ\text{C}/\text{min}$, and the crystallization morphology evolution during the cooling process was observed. The thermal stability of the samples was checked using an STA analyzer (TGA/DSC3+, Mettler Toledo, Switzerland) from the temperature range of $50\text{--}500^\circ\text{C}$ with a heating rate of $10^\circ\text{C}/\text{min}$ under the nitrogen atmosphere. Differential scanning calorimetry (DSC) measurement was performed on a TA-DSC calorimeter (PE, Mettler Toledo, Zurich, Switzerland) under a nitrogen flow of $50 \text{ mL}/\text{min}$. To eliminate the thermal history of the nanocomposite samples, the samples were heated from 20°C to 200°C at a heating rate of $10^\circ\text{C}/\text{min}$ under a nitrogen atmosphere for 5 min . Then, the melt was cooled to 20°C at a rate of $10^\circ\text{C}/\text{min}$ and reheated to 200°C . The first cooling and second heating scan curves were recorded.

Rat bone marrow mesenchymal stem cells (BMSCs) were used as model cells. Cell Counting Kit (CCK-8) was used to evaluate the cell adhesion and proliferation capacity of neat PLLA, PLLA/SLG, and PLLA/GNS. After BMSCs ($20,000 \text{ cells}/\text{cm}^2$) had been seeded on the surface of the nanocomposites and cultured for 1 day and 3 days , the solution of CCK-8 (Dojingdo Laboratories, Kumamoto, Japan) with a concentration ratio of $1:10$ to the culture medium was added. Then, after the cells were incubated in an atmosphere of $5\% \text{ CO}_2$ and 37°C for 2 h , the optical density (OD) of the solution was measured at 450 nm with a microplate reader (Multiskan MK3, Thermo Fisher Scientific, Shanghai, China). The contact angle test was used to evaluate the hydrophilicity and hydrophobicity of material surfaces (OCA 20, Dataphysics, Stuttgart, Germany). Contact angles reported are the average of at least three measurements per sample.

3. Results and Discussion

3.1. Composition, Structure and Morphology of the Nanocomposite Films

The compositions of neat PLLA and representative PLLA/SLG (PSG) and PLLA/GNS (PGN) composites at the same mass ratio were determined by confocal laser Raman spectroscopy (Figure 1). Different from pure PLLA, exhibiting characteristic bands at 2940 cm^{-1} identified as C-H stretching modes of $-\text{CH}_3$ groups (Figure 1a,b), new bands appeared in the Raman spectra of PSG and PGN, with wavelengths around 1580 cm^{-1} and 2700 cm^{-1} , corresponding to the G and 2D peaks of graphene (Figure 1a,b). Combined with the I_G/I_{2D} value of each composite material around $1:1$ (Figure 1a,b), it can be seen that the graphene in the composite material is complete and uniformly dispersed. Fully confirmed the effective combination of SLG and PLLA, and GNS dispersed in the PLLA matrix. In addition, the appearance of graphene D peaks was not observed, indicating that the structures of the obtained SLG and GNS were complete and defect-free.

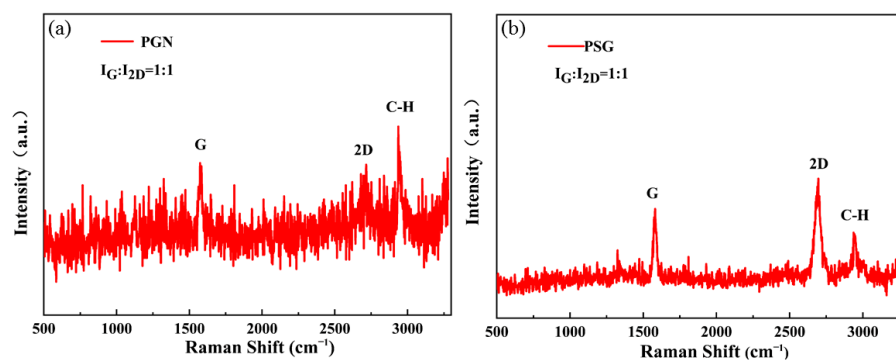


Figure 1. Raman spectra of (a) PSG and (b) PGN nanocomposites with the same $M_{\text{PLLA}}/M_{\text{Graphene}}$.

To characterize the morphology and dispersion of SLG and GNS in the composites, SEM images of PLLA, PSG, and PGN composite films were studied (Figure 2). Because of the various types and adding procedures of graphene, the surface of each film was unique. The surface of the composite film added with SLG was comparable to that surface of neat PLLA, with dense and fine dendrites distributed (Figure 2a,b). The addition of GNS will make the dendrites on the surface of the film connected to a certain extent, resulting in a thicker crystalline surface (Figure 2c). This might originate from the interfacial interaction between GNS and PLLA. It was also consistent with the subsequent crystallization test. It is worth mentioning, however, that because of the limited compatibility of GNS with the PLLA matrix, there were some GNS aggregation on the surface indicated by the red arrows (Figure 2c).

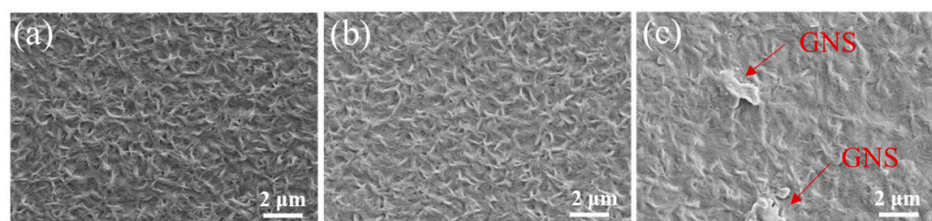


Figure 2. SEM images of surface morphologies of (a) neat PLLA (b) PSG and (c) PGN composites films.

3.2. Crystallization Behavior of the Nanocomposites

The crystallinity of a polymer plays a crucial role in its performance. As a semi-crystalline polymer, it is very meaningful to study the crystallization of PLLA and the effect of SLG and GNS as fillers on its crystallization behavior. The XRD patterns of nanocomposite films including pure PLLA, PSG, and PGN are shown in Figure 3. In general, crystals with two different structures, α , and β , can be detected in PLLA. The diffraction patterns of pure PLLA, PSG, and PGN in Figure 3 all have the strongest diffraction peaks at $2\theta = 16.5^\circ$, corresponding to the (110) and (200) reflections of PLLA, which indicate that PLLA in nanocomposites is in the order of orthorhombic α -crystal form exists [38]. Moreover, less intense diffraction peaks were observed at 18.7° and 21.7° , corresponding to the (203) and (210) reflections of PLLA, respectively. The creation of a few mesomorphic structures in the PLLA due to an excessive cooling rate is primarily responsible for the appearance of these peaks [39,40]. All XRD patterns revealed the same diffraction peaks, which means that the incorporation of SLG and GNS did not change the crystal structure of PLLA in the nanocomposites. Interestingly, the diffraction peak intensity of PLLA was significantly increased in PSG and PGN nanocomposites, indicating an improvement in crystallinity and an increase in crystal order [41]. In addition, as shown in Figure 3, in the XRD patterns of PSG and PGN, the characteristic diffraction peak at 26.5° attributed to graphite was not detected, indicating that the dispersion of graphene in the PLLA matrix was good and close to the monolayer level, which was consistent with the results of Raman spectroscopy.

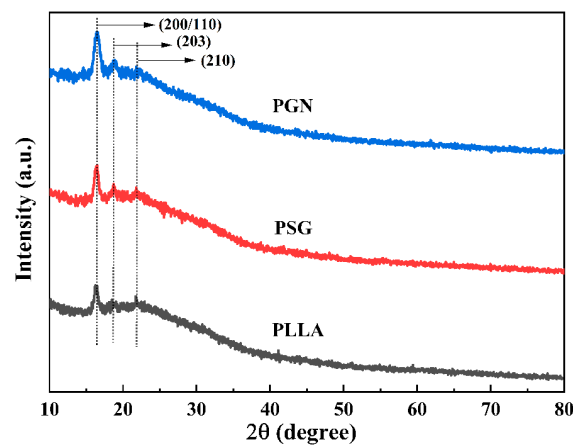


Figure 3. XRD patterns of neat PLLA, PSG and PGN nanocomposite films.

Since PLLA is a semicrystalline polymer, the mechanical properties are influenced by the degree of the crystallinity to some extent [42,43]. DSC was used to investigate the crystallization behavior of PLLA in the nanocomposite. Figure 4 showed the DSC heating and cooling curves of the neat PLLA, PSG and PGN nanocomposites at a scan rate of 10 °C/min, and the results of typical thermal properties, including T_g (glass transition temperature), T_c (cold crystallization temperature), T_m (melting point temperature), ΔH_c (the cold crystallization enthalpy and χ_c (the crystallinity) were listed in Table 1. The degree of crystallization of the films was calculated by the following Equation (1),

$$\chi_c = \left(\frac{\Delta H_c}{\Delta H_m^0} \right) \times 100\% \quad (1)$$

where χ_c is the percent crystallinity, ΔH_c was the enthalpy of the cold crystallization of nanocomposites, and ΔH_m^0 was the enthalpy of the melting with a value of 93.0 J/g, which was reported to be the melting enthalpy for 100% crystalline PLLA [44]. With the existence of SLG and GNS, the exothermic peaks become more noticeable and ΔH_c was higher. Furthermore, at the same mass ratio of graphene filling, PSG nanocomposites have distinct and sharper exothermic peaks than PGN nanocomposites. This is because graphene provides PLLA with heterogeneous nucleation sites, which improves the crystallization ability of PLLA, and the nucleation speed of SLG is faster than that of GNS. Both T_c and χ_c of the nanocomposites were significantly increased after the addition of SLG and GNS, indicating that the presence of SLG and GNS favored the non-isothermal cold crystallization behavior of PLLA due to the efficient nucleating effect of graphene for PLLA crystallization. For polymers, the high molecular mobility at high temperatures is very beneficial for crystal nucleation. In the presence of graphene, the exothermic amplitude of PLLA crystals increases and the crystallization exotherm sharpens, meaning that both crystallization nucleation and crystal growth of the PLLA matrix are enhanced. Ajala et al. [40] likewise came up with similar findings. The increased T_g values of PSG and PGN nanocomposites can be attributed to the effective linkage of PLLA to graphene that restricts the segmental motion of PLLA chains, and this increased stability also indicates a higher interfacial bond strength between PLLA and graphene [45]. Further, a rise in T_m in nanocomposites suggested that SLG and GNS are beneficial to the perfection of crystallites and prevent the formation of more defective PLLA crystallites.

Table 1. Calorimetric data derived from the DSC cooling curves and heating curves for the PLLA, PSG and PGN nanocomposites.

Samples	T_g (°C)	T_c (°C)	T_m (°C)	ΔH_c (J/g)	χ_c (%)
PLLA	60.4	116.9	176.5	33.4	35.9
PSG	62.1	132.2	177.6	38.0	40.9
PGN	65.3	122.8	178.6	39.6	42.6

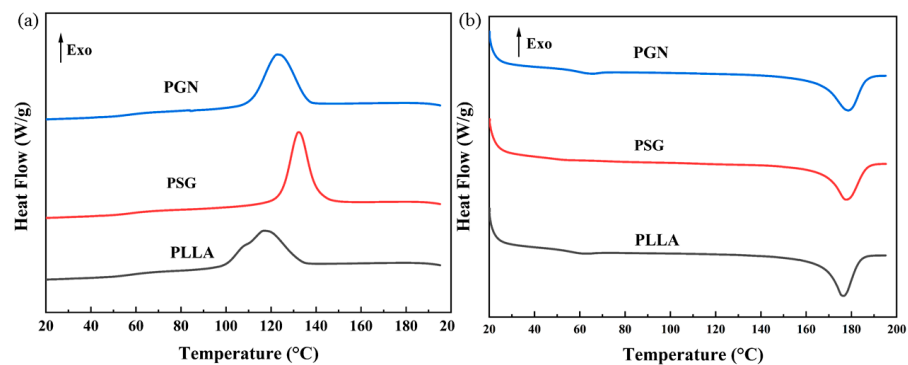


Figure 4. DSC curves of (a) the cooling curves and (b) the heating curves of PLLA, PSG and PGN nanocomposites with different filler contents.

To further specifically explore the nucleation effect of graphene on PLLA crystallization, polarizing microscopy (POM) was used to study the isothermal crystallization morphologies of neat PLLA and its nanocomposites at around their crystallization temperatures (120, 127 and 136 °C, respectively). Figure 5 showed the spherulitic morphology of neat PLLA, PSG, and PGN at different crystallization times. Only a few nuclei appear in neat PLLA whereas PSG and PGN show more nuclei after 1 min (Figure 5a,d,g). The morphological differences for PLLA, PSG, and PGN are more obvious after 5 min (Figure 5c,f,i). For neat PLLA, the number of spherulites is small, and their size is relatively big because the spherulites had large space to grow before impinging on each other (Figure 5c). With the addition of graphene, the number of PLLA spherulites increases significantly, and consequently, their size is dramatically reduced (Figure 5f,i). Spherulitic morphology studies here clearly suggest the strong heterogeneous nucleation effect of graphene, which is in agreement with DSC findings.

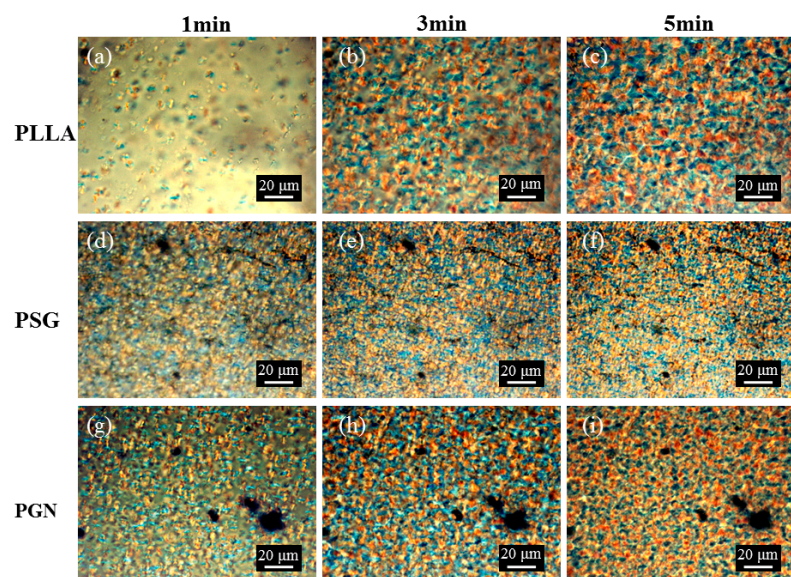


Figure 5. Polarized optical micrographs for 1 min, 3 min and 5 min of (a–c) neat PLLA isothermally crystallized at 120 °C (d–f) PSG nanocomposite isothermally crystallized at 136 °C (g–i) and PGN nanocomposite isothermally crystallized at 127 °C.

3.3. Mechanical, Thermal Properties and Biocompatibility

Considering the remarkable mechanical properties of graphene, such as high mechanical strength and high modulus, it is predicted that the mechanical properties of PLLA nanocomposites will be enhanced by SLG and GNS. The mechanical properties of pure PLLA, PSG, and PGN nanocomposite films were evaluated using tensile tests,

and typical stress-strain curves are shown in Figure 6a. The variations of tensile strength, Young's modulus, and elongation at break are plotted in Figure 6b–d. As seen in Figure 6a, all nanocomposite films show a typical characteristic of ductile fracture behavior with a well-defined yield point, including the neat PLLA films. While as a brittle material, the reason why neat PLLA exhibit a typical characteristic of ductile fracture behavior may be due to the incomplete discharge of the dissolving agent. Nevertheless, some significant changes can be observed in the mechanical properties of polymer by graphene. The tensile strength and Young's modulus of PSG nanocomposite films were significantly increased as compared to that of neat PLLA film (30.47 MPa and 1.13 GPa), and reached a maximum of 40.45 MPa and 1.31 GPa (Figure 6a,b), indicating that the mechanical strength of PSG nanocomposite films is enhanced. Different from the previous study [46], the toughness of PSG was also improved compared with that of neat PLLA film, and the elongation at break increased from 114.07% to 123.95%. The reason for this simultaneous improvement of mechanical strength and toughness is mainly attributed to the good interfacial interaction between SLG and PLLA matrix. Meanwhile, GNS greatly improves the toughness of PGN nanocomposite films based on sacrificing some mechanical strength, and the elongation at break increases to 204.97%, an increase of 79.7%. (Figure 6d). Compared with neat PLLA, SLG can play the role of strengthening and toughening at the same time, while GNS can greatly improve stretch ability with low content. Therefore, choosing different kinds of graphene as reinforcing fillers has different effects, which is consistent with many previous reports of nanofiller-reinforced PLLA composites [47,48]. This result may be attributed to the different interfacial structures between nanofillers and polymer matrix.

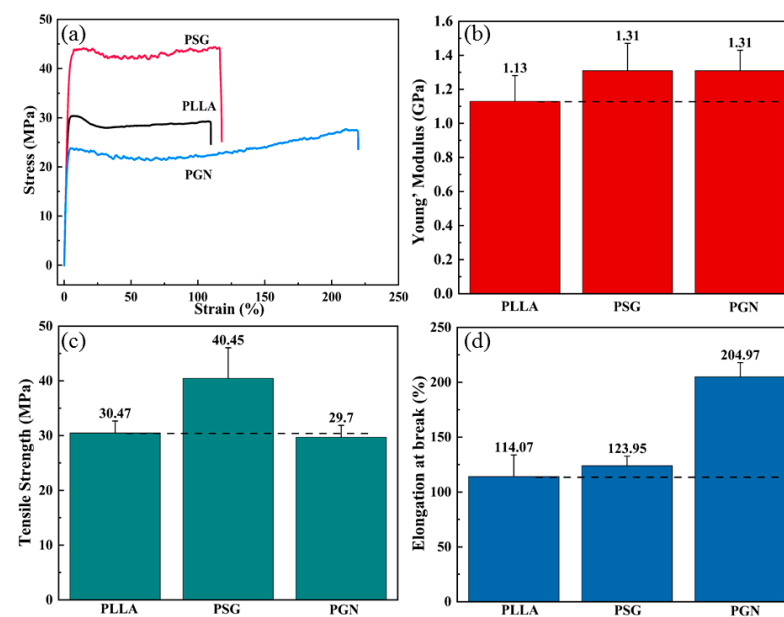


Figure 6. (a) Representative stress-strain curves for PLLA, PSG, PGN nanocomposite films; the variations of (b) Young's modulus, (c) tensile strength, (d) elongation at break as a function of PLLA number of layers.

In fact, the improvement in tensile strength and tensile modulus depends on factors such as the shape and dispersion of nanofillers in the matrix, nanofillers interfacial adhesion, and strength with the matrix material. However, the shape and dispersion of graphene play an important role in the enhancement of the tensile properties of PLLA. In PSG, the SLG is composited with the polylactic acid matrix in the mode of whole-sheet coverage, and the compatibility between SLG-PLLA acid and PLLA matrix is stronger, so the effective contact area between the nanofiller and the matrix is larger, and the adhesion energy is higher. When the composite nanomaterials are subjected to stress stretching, SLG can limit the expansion of cracks, avoid the formation of larger cracks, and improve the tensile strength

of the composites. In addition, SLG also restricts the mobility of polymer chains under load by blocking the molecular chains. The increased crosslinking rate in the PLLA matrix and the restricted movement of the PLLA macromolecular chains ultimately improved the tensile modulus of the nanocomposite PSG. From the shape and dispersibility of nanofillers, GNS are complexed in the matrix in the form of small clusters. Due to the strong van der Waals forces between GNS, GNS are more likely to accumulate in the matrix and have poorer dispersion. The interfacial interaction force between GNS and PLLA is weaker, which also leads to a slight decrease in the strength of PGN. Therefore, the good interfacial interaction between SLG and PLLA can effectively transfer the load to SLG, enhancing the tensile strength and tensile modulus of PLLA/graphene nanocomposites.

On the other hand, since PLLA is semi-crystalline, including the interfacial interaction between the nanofillers and the polymer matrix, the crystal structure, and morphology of the polymer matrix are also key factors affecting the mechanical properties of nanocomposites. The results of XRD (Figure 3), DSC (Figure 4), and POM (Figure 5) confirmed that the addition of SLG and GNS both improved the crystallinity of PLLA, and benefited from the excellent heterogeneous nucleating ability of graphene on PLLA crystallization. The nanofiller-induced interfacial crystallization layer plays a key role in the non-covalent stress transfer between graphene and PLLA. As mentioned earlier, the larger contact area between SLG and PLLA matrix results in the formation of a larger interfacial crystalline layer, which can lead to a significant increase in mechanical strength. The addition of SLG and GNS not only improved the crystallinity of the nanocomposites, but also tended to induce the PLLA matrix to form spherulites with smaller diameters. It is very important for the improvement of toughness. In general, unreinforced amorphous polymers undergo plastic deformation through unhindered shear band propagation. The fine-grained PLLA crystals in PSG and PGN provide resistance to the propagation of shear bands, thus, the plasticity of the nanocomposites is greatly enhanced. Especially in the PGN nanocomposites with the highest crystallinity and the smallest spherulite size, this toughness enhancement is extremely obvious.

Aliphatic polyesters such as PLLA in particular are easy to hydrolyze and thermally degrade to monomers and oligomers, improving the thermal stability of PLLA an important part as regards processing. It was found that the incorporation of SLG and GNS not only improved the mechanical properties of PLLA, but also enhanced its thermal stability. Figure 7 and Table 2 show the TGA and corresponding differential thermogravimetric analysis (DTA) results of the neat PLLA, PSG, and PGN composite films. In PSG and PGN nanocomposites, the decomposition onset temperature (T_{onset}), the maximum decomposition temperature (T_{max}), and the decomposition temperature at 50% weight loss (T_{50}) of the composite films shifted to higher temperatures. Among them, the decomposition onset temperature and maximum decomposition temperature of PSG were observed to vary from 267 °C to 271 °C and from 348 °C to 349 °C, respectively. The improved thermal stability is mainly due to the presence of SLG and GNS as reinforcing fillers, they can delay oxygen permeation and volatile degradation products escape and coke formation by the so-called “tortuous path” effect of graphene [49]. Moreover, it can be seen from the DTA curves that the DTA peaks of PGN and PSG are higher in temperature than that of neat PLLA. This change can be ascribed that when PLLA is heated, free radicals are generated which cause the degradation of the PLLA matrix. The increase in the crystallinity of PSG and PGN makes the degradation rate slower, and the degradation requires more energy, so the degradation temperature is also higher [50]. Therefore, good interfacial interaction and high crystallinity also contribute to the thermal stability of PLLA nanocomposites.

Table 2. Thermal data derived from the TGA curves and DTA curves of neat PLLA, PSG and PGN nanocomposites.

Samples	T_{onset} (°C)	T_{max} (°C)	T_{50} (°C)
PLLA	267	354	348
PSG	271	355	349
PGN	259	357	350

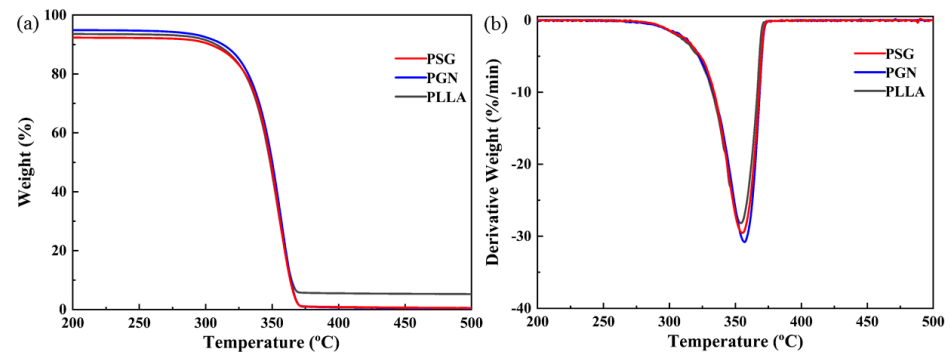


Figure 7. (a) TGA and (b) DTA curves for neat PLLA, PSG and PGN nanocomposite.

From the results obtained above, the fact can be known that SLG and GNS can be used to improve the mechanical properties and thermal stability of PLLA, but the biocompatibility of the composites determines whether PLLA/graphene nanocomposites can be used for the preparation of biomedical materials. The biocompatibility of the nanocomposites was evaluated by the CCK-8 test (Figure 8). All samples were $0.5 \times 0.5 \text{ cm}^2$ in size. Rat bone marrow mesenchymal stem cells (BMSCs) were inoculated and cultured for 1 day and 3 days. As shown in Figure 8, the OD values of PSG and PGN increased slightly after 1 day of culture. But after 3 days, it was found that the OD values of the PLLA/SLG and PLLA/GNS groups were significantly higher than those of the neat PLLA group, indicating that the cells on the surface of the nanocomposites are more than that of neat PLLA. This may benefit from the improvement of SLG and GNS on the surface of the nanocomposites, and the hydrophilic surface improves the cell proliferation ability. From the contact angle test results, the contact of a pure PLLA film was $94.3^\circ (\pm 1.7^\circ)$. However, after adding a layer of single-layer graphene, the contact angle of the PSG surface was reduced to $88.3^\circ (\pm 1.4^\circ)$, and the hydrophilicity of the surface was further improved. Meanwhile, there was a small-decreased contact angle of PGN ($91.2^\circ \pm 0.7^\circ$), and all the results revealed the surface of the nanocomposite materials is hydrophilic. All these tests proved that the existence of SLG and GNS provided a good adhesion environment for cells, which is conducive to cell proliferation and has good cell activity.

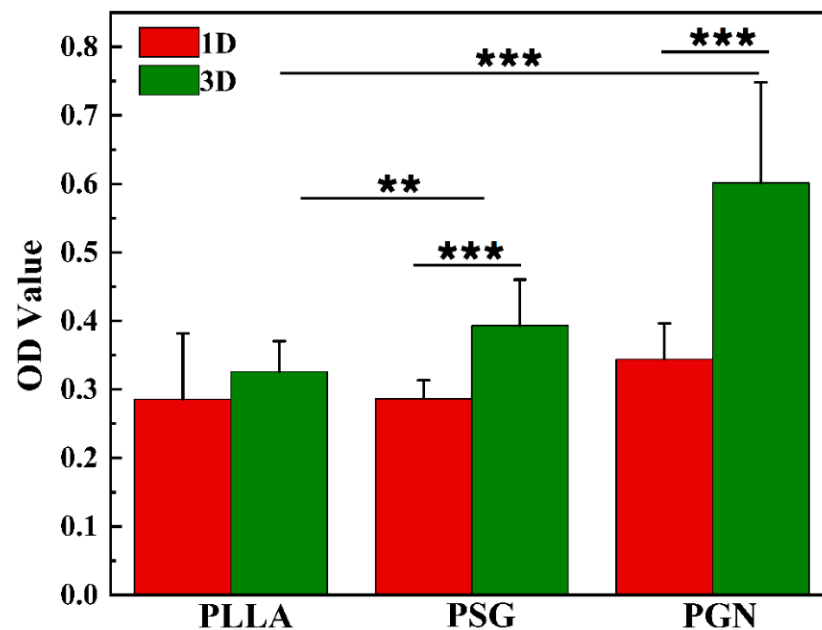


Figure 8. Cell viability measured with CCK-8 assay on PLLA, PSG and PGN nanocomposites monolayer film at different culture times (** $p < 0.01$, *** $p < 0.001$).

4. Conclusions

In this paper, two kinds of graphene, single-layer graphene (SLG) and graphene nanosheets (GNS), and poly L-lactic acid (PLLA) nanocomposite membranes were successfully prepared. The effects of SLG and GNS on the mechanical properties, crystallization ability, thermal stability, and cell viability of PLLA nanocomposites were investigated.

SLG and GNS act as nucleating agents to further enhance the crystallinity of PLLA. The good interaction between SLG and PLLA matrix makes PSG have high mechanical strength. Moreover, SLG and GNS greatly improve the toughness of PGN by changing the shape and crystallinity of PLLA crystal. The tensile strength and fracture toughness of PSG were increased by 32.8% and 8.7% respectively, and the toughness of PGN was increased by 79.7%.

In addition, CCK-8 results indicated that PSG and PGN were non-cytotoxic, and the nanocomposite membranes showed good cell survival and proliferation ability. These PSG and PGN nanocomposites with higher mechanical properties, thermal stability, and cell viability exhibit broad application prospects as biomedical materials.

Author Contributions: Y.H.: conceptualization, methodology, writing—original draft preparation; J.Y.: writing—review and editing and funding acquisition; K.C.: conceptualization, methodology, writing—review and editing, supervision, project administration; X.H.: formal analysis and investigation; W.W.: writing—review and editing. All authors have read and agreed to the published version of the manuscript.

Funding: This research was supported by the Natural Science Foundation of Zhejiang Province of China (Grant no. LGF20H030009).

Institutional Review Board Statement: Not applicable.

Informed Consent Statement: Not applicable.

Data Availability Statement: Not applicable.

Conflicts of Interest: The authors declare no conflict of interest.

References

1. Nampoothiri, K.M.; Nair, N.R.; John, R.P. An overview of the recent developments in polylactide (PLLA) research. *Bioresour. Technol.* **2010**, *101*, 8493–8501. [[CrossRef](#)] [[PubMed](#)]
2. Saeidlou, S.; Huneault, M.A.; Li, H.B.; Park, C.B. Poly(lactic acid) crystallization. *Prog. Polym. Sci.* **2012**, *37*, 1657–1677. [[CrossRef](#)]
3. Savaris, M.; Santos, V.D.; Brandalise, R.N. Influence of different sterilization processes on the properties of commercial poly(lactic acid). *Mater. Sci. Eng. C* **2016**, *69*, 661–667. [[CrossRef](#)] [[PubMed](#)]
4. Yang, F.; Murugan, R.; Ramakrishna, S.; Wang, X.; Ma, Y.X.; Wang, S. Fabrication of nanostructured porous PLLA scaffold intended for nerve tissue engineering. *Biomaterials* **2005**, *25*, 1891–1900. [[CrossRef](#)] [[PubMed](#)]
5. John, R.P.; Nampoothiri, K.M.; Pandey, A. Solid-state fermentation for L-lactic acid production from agro wastes using *Lactobacillus delbrueckii*. *Proc. Biochem.* **2006**, *41*, 759–763. [[CrossRef](#)]
6. Singhvi, M.S.; Zinjarde, S.S.; Gokhale, D.V. Polylactic acid: Synthesis and biomedical applications. *J. Appl. Microbiol.* **2019**, *127*, 1612–1626. [[CrossRef](#)]
7. Guerra, A.J.; Cano, P.; Rabionet, M.; Puig, T.; Ciurana, J. 3D-Printed PCL/PLLA Composite Stents: Towards a New Solution to Cardiovascular Problems. *Materials* **2018**, *11*, 1679. [[CrossRef](#)]
8. Zhang, B.Q.; Wang, L.; Song, P.; Pei, X.; Sun, H.; Wu, L.A.; Zhou, C.C.; Wang, K.F.; Fan, Y.J.; Zhang, X.D. 3D printed bone tissue regenerative PLLA/HA scaffolds with comprehensive performance optimizations. *Mater. Des.* **2021**, *201*, 109490. [[CrossRef](#)]
9. Liu, S.Q.; Yu, J.J.; Li, H.M.; Wang, K.W.; Wu, G.H.; Wang, B.W.; Liu, M.F.; Zhang, Y.; Wang, P.; Zhang, J. Controllable Drug Release Behavior of Poly(lactic acid) (PLLA) Surgical Suture Coating with Ciprofloxacin (CPFX)-Polycaprolactone (PCL)/Polyglycolide (PGA). *Polymers* **2020**, *12*, 288. [[CrossRef](#)]
10. Rasal, R.M.; Janorkar, A.V.; Hirt, D.E. Poly(lactic acid) modifications. *Prog. Polym. Sci.* **2010**, *35*, 338–356. [[CrossRef](#)]
11. Lim, L.T.; Auras, R.; Rubino, M. Processing technologies for poly(lactic acid). *Prog. Polym. Sci.* **2008**, *33*, 820–852. [[CrossRef](#)]
12. Bharadwaz, A.; Jayasuriya, A.C. Recent trends in the application of widely used natural and synthetic polymer nanocomposites in bone tissue regeneration. *Mater. Sci. Eng. C-Mater.* **2020**, *110*, 110698. [[CrossRef](#)]
13. Terzopoulou, Z.; Klonos, P.A.; Kyritsis, A.; Tziolas, A.; Avgeropoulos, A.; Papageorgiou, G.Z.; Bikiaris, D.N. Interfacial interactions, crystallization and molecular mobility in nanocomposites of Poly(lactic acid) filled with new hybrid inclusions based on graphene oxide and silica nanoparticles. *Polymer* **2019**, *166*, 1–12. [[CrossRef](#)]

14. Raquez, J.M.; Murena, Y.; Goffin, A.L.; Habibi, Y.; Ruelle, B.; DeBuyl, F.; Dubois, P. Surface-modification of cellulose nanowhiskers and their use as nanoreinforcers into polylactide: A sustainably-integrated approach. *Compos. Sci. Technol.* **2012**, *72*, 544–549. [[CrossRef](#)]
15. Li, Y.C.; Liao, C.Z.; Tjong, S.C. Synthetic Biodegradable Aliphatic Polyester Nanocomposites Reinforced with Nanohydroxyapatite and/or Graphene Oxide for Bone Tissue Engineering Applications. *Nanomaterials* **2019**, *9*, 590. [[CrossRef](#)]
16. Bai, T.T.; Zhu, B.; Liu, H.; Wang, Y.M.; Song, G.; Liu, C.T.; Shen, C.Y. Biodegradable poly(lactic acid) nanocomposites reinforced and toughened by carbon nanotubes/clay hybrids. *Int. J. Biol. Macromol.* **2019**, *151*, 628–634. [[CrossRef](#)] [[PubMed](#)]
17. Xia, S.; Liu, X.B.; Wang, J.F.; Kan, Z.; Chen, H.; Fu, W.X.; Li, Z.B. Role of poly(ethylene glycol) grafted silica nanoparticle shape in toughened PLLA-matrix nanocomposites. *Compos. B Eng.* **2019**, *168*, 398–405. [[CrossRef](#)]
18. Mayekar, P.C.; Castro-Aguirre, E.; Auras, R.; Selke, S.; Narayan, R. Effect of Nano-Clay and Surfactant on the Biodegradation of Poly(Lactic Acid) Films. *Polymers* **2020**, *12*, 311. [[CrossRef](#)]
19. Liu, X.Z.; He, X.; Jin, D.W.; Wu, S.T.; Wang, H.S.; Yin, M.; Aldalbahi, A.; El-Newehy, M.; Mo, X.M.; Wu, J.L. A biodegradable multifunctional nanofibrous membrane for periodontal tissue regeneration. *Acta Biomater.* **2020**, *108*, 207–222. [[CrossRef](#)]
20. Wu, S.H.; Zhou, R.; Zhou, F.; Streubel, P.N.; Chen, S.J.; Duan, B. Electrospun thymosin Beta 4 loaded PLGA/PLLA nanofiber/microfiber hybrid yarns for tendon tissue engineering application. *Mater. Sci. Eng. C-Mater.* **2020**, *106*, 110268. [[CrossRef](#)]
21. Tan, Y.J.; Li, J.; Tang, X.H.; Yue, T.N.; Wang, M. Effect of phase morphology and distribution of multi-walled carbon nanotubes on microwave shielding of poly(L-lactide)/poly(epsilon-caprolactone) composites. *Compos. Part A-Appl. Sci. Manuf.* **2020**, *137*, 106008. [[CrossRef](#)]
22. Yang, H.T.; Shi, B.B.; Xue, Y.J.; Ma, Z.W.; Liu, L.N.; Liu, L.; Yu, Y.M.; Zhang, Z.Y.; Annamalai, P.K.; Song, P.A. Molecularly Engineered Lignin-Derived Additives Enable Fire-Retardant, UV-Shielding, and Mechanically Strong Polylactide Biocomposites. *Biomacromolecules* **2021**, *22*, 1432–1444. [[CrossRef](#)] [[PubMed](#)]
23. Novoselov, K.S.; Geim, A.K.; Morozov, S.V.; Jiang, D.; Zhang, Y.; Dubonos, S.V.; Grigorieva, I.V.; Firsov, A.A. Electric field effect in atomically thin carbon films. *Science* **2004**, *306*, 666–669. [[CrossRef](#)]
24. Korkmaz, S.; Kariper, I.A. Graphene and graphene oxide based aerogels: Synthesis, characteristics and supercapacitor applications. *J. Energy Storage* **2020**, *27*, 101038. [[CrossRef](#)]
25. Afroj, S.; Tan, S.R.; Abdelkader, A.M.; Novoselov, K.S.; Karim, N. Highly Conductive, Scalable, and Machine Washable Graphene-Based E-Textiles for Multifunctional Wearable Electronic Applications. *Adv. Funct. Mater.* **2020**, *30*, 2000293. [[CrossRef](#)]
26. Cao, K.; Feng, S.Z.; Han, Y.; Gao Ly, T.H.; Xu, Z.P.; Lu, Y. Elastic straining of free-standing monolayer graphene. *Nat. Commun.* **2020**, *11*, 284. [[CrossRef](#)] [[PubMed](#)]
27. Bie, C.B.; Yu, H.G.; Cheng, B.; Ho, W.; Fan, J.J.; Yu, J.G. Design, Fabrication, and Mechanism of Nitrogen-Doped Graphene-Based Photocatalyst. *Adv. Mater.* **2021**, *33*, 2003521. [[CrossRef](#)]
28. Dai, W.; Lv, L.; Ma, T.F.; Wang, X.Z.; Ying, J.F.; Yan, Q.W.; Tan, X.; Gao, J.Y.; Xue, C.; Yu, J.H. Multiscale Structural Modulation of Anisotropic Graphene Framework for Polymer Composites Achieving Highly Efficient Thermal Energy Management. *Adv. Sci.* **2021**, *8*, 2003734. [[CrossRef](#)]
29. Raslam, A.; del Burgo, L.S.; Ciriza, J.; Pedraz, J.L. Graphene oxide and reduced graphene oxide-based scaffolds in regenerative medicine. *Int. J. Pharmaceut.* **2020**, *580*, 119226. [[CrossRef](#)]
30. Liang, J.J.; Huang, Y.; Zhang, L.; Wang, Y.; Ma, Y.F.; Guo, T.Y.; Chen, Y.S. Molecular level dispersion of graphene into poly(vinyl alcohol) and effective reinforcement of their nanocomposites. *Adv. Funct. Mater.* **2009**, *19*, 2297–2302. [[CrossRef](#)]
31. Cheng, H.K.F.; Sahoo, N.G.; Tan, Y.P.; Pan, Y.Z.; Bao, H.Q.; Li, L.; Chan, S.H.; Zhao, J.H. Poly(vinyl alcohol) nanocomposites filled with poly(vinyl alcohol)-grafted graphene oxide. *ACS Appl. Mater. Interfaces* **2012**, *4*, 2387–2394. [[CrossRef](#)] [[PubMed](#)]
32. Zakaria, M.R.; Kudus, M.H.A.; Akil, H.M.; Thirmizir, M.Z.M.; Malik, M.F.I.A.; Othman, M.B.H.; Ullah, F.; Javed, F. Comparative Study of Single-Layer Graphene and Single-Walled Carbon Nanotube-Filled Epoxy Nanocomposites Based on Mechanical and Thermal Properties. *Polym. Compos.* **2019**, *40*, 1840–1849. [[CrossRef](#)]
33. Caminero, M.A.; Chacon, J.M.; Garcia-PLLAza, E.; Nunez, P.J.; Reverte, J.M.; Becar, J.P. Additive Manufacturing of PLLA-Based Composites Using Fused Filament Fabrication: Effect of Graphene NanoPLLAtelet Reinforcement on Mechanical Properties, Dimensional Accuracy and Texture. *Polymers* **2019**, *11*, 799. [[CrossRef](#)] [[PubMed](#)]
34. Yang, L.; Zhen, W.J. Poly(lactic acid)/p-phenylenediamine functionalized graphene oxidized nanocomposites: Preparation, rheological behavior and biodegradability. *Eur. Polym. J.* **2019**, *121*, 109341. [[CrossRef](#)]
35. Mao, N.D.; Jeong, H.; Nguyen, T.K.N.; Nguyen, T.M.L.; Do, T.V.V.; Thuc, C.N.H.; Perre, P.; Ko, S.C.; Kim, H.G.; Tran, D.T. Polyethylene glycol functionalized graphene oxide and its influences on properties of Poly(lactic acid) biohybrid materials. *Compos. B Eng.* **2019**, *161*, 651–658. [[CrossRef](#)]
36. Liu, Y.S.; Chen, T.; Du, F.; Gu, M.; Zhang, P.; Zhang, X.; Liu, J.Z.; Lv, L.W.; Xiong, C.Y.; Zhou, Y.S. Single-Layer Graphene Enhances the Osteogenic Differentiation of Human Mesenchymal Stem Cells In Vitro and In Vivo. *J. Biomed. Nanotechnol.* **2016**, *12*, 1270–1284. [[CrossRef](#)]
37. Long, X.J.; Wang, X.Z.; Yao, L.L.; Lin, S.Y.; Zhang, J.M.; Weng, W.J.; Cheng, K.; Wang, H.M.; Lin, J. Graphene/Si-Promoted Osteogenic Differentiation of BMSCs through Light Illumination. *ACS Appl. Mater. Interfaces* **2019**, *11*, 43857–43864. [[CrossRef](#)]
38. Hoogsteen, W.; Postema, A.R.; Pennings, A.J.; Ten Brinke, G.; Zugenmaier, P. Crystal structure, conformation and morphology of solution spun poly(L-lactide) fibers. *Macromolecules* **1990**, *23*, 634–642. [[CrossRef](#)]

39. Stoclet, G.; Seguela, R.; Lefebvre, J.M.; Rochas, C. New insights on the strain-induced mesophase of poly(D, L-lactide):in situ WAXS and DSC study of the thermos-mechanical stability. *Macromolecules* **2010**, *43*, 7228–7237. [[CrossRef](#)]
40. Bao, C.L.; Song, L.; Xing, W.Y.; Yuan, B.H.; Wilkie, C.A.; Huang, J.L.; Guo, Y.Q.; Hu, Y. Preparation of graphene by pressurized oxidation and multiplex reduction and its polymer nanocomposites by masterbatch-based melt blending. *J. Mater. Chem.* **2012**, *22*, 6088–6096. [[CrossRef](#)]
41. Harris, A.M.; Lee, E.C. Improving mechanical performance of injection molded PLLA by controlling crystallinity. *J. Appl. Polym. Sci.* **2008**, *107*, 2246–2255. [[CrossRef](#)]
42. Yin, H.Y.; Wei, X.F.; Bao, R.Y.; Dong, Q.X.; Liu, Z.Y.; Yang, W.; Xie, B.H.; Yang, M.B. Enhancing thermomechanical properties and heat distortion resistance of poly(l-lactide) with high crystallinity under high cooling rate. *ACS Sustain. Chem. Eng.* **2015**, *3*, 654–661. [[CrossRef](#)]
43. Kalb, B.; Pennings, A.J. General crystallization behavior of poly(L-lactic acid). *Polymer* **1980**, *21*, 607–612. [[CrossRef](#)]
44. Ajala, O.; Werther, C.; Nikaeen, P.; Singh, R.P.; Depan, D. Influence of graphene nanoscrolls on the crystallization behavior and nano-mechanical properties of polylactic acid. *Polym. Adv. Technol.* **2019**, *30*, 1825–1835. [[CrossRef](#)]
45. Li, W.X.; Xu, Z.W.; Chen, L.; Shan, M.J.; Tian, X.; Yang, C.Y.; Lv, H.M.; Qian, X.M. A facile method to produce graphene oxide-g-poly(L-lactic acid) as a promising reinforcement for PLLA nanocomposites. *Chem. Eng. J.* **2014**, *237*, 291–299. [[CrossRef](#)]
46. Tsuji, H.; Aratani, T.; Takikawa, H. Physical properties, crystallization, and thermal/hydrolytic degradation of poly(L-lactide)/nano/micro-diamond composites. *Macromol. Mater. Eng.* **2013**, *298*, 1149–1159. [[CrossRef](#)]
47. Kim, I.H.; Jeong, Y.G. Polylactide/exfoliated graphite nanocomposites with enhanced thermal stability, mechanical modulus, and electrical conductivity. *J. Polym. Sci. Part B* **2010**, *48*, 850–858. [[CrossRef](#)]
48. Duan, J.K.; Shao, S.X.; Li, Y.; Wang, L.F.; Jiang, P.K.; Liu, B.P. Polylactide/graphite nanosheets/MWCNTs nanocomposites with enhanced mechanical, thermal and electrical properties. *Iran. Polym. J.* **2012**, *21*, 109–120. [[CrossRef](#)]
49. McLauchlin, A.R.; Thomas, N.L. Preparation and thermal characterization of poly(lactic acid) nanocomposites prepared from organoclays based on an amphoteric surfactant. *Polym. Degrad. Stabil.* **2009**, *94*, 868–872. [[CrossRef](#)]
50. Ramanathan, T.; Abdala, A.A.; Stankovich, S.; Dikin, D.A.; Herrera-Alonso, M.; Piner, R.D.; Adamson, D.H.; Schniepp, H.C.; Chen, X.; Ruoff, R.S. Functionalized graphene sheets for polymer nanocomposites. *Nat. Nanotechnol.* **2008**, *3*, 327–331. [[CrossRef](#)]